3D Printing of Magnetoresponsive Polymeric Materials with Tunable Mechanical and Magnetic Properties by Digital Light Processing

S. Lantean, G. Barrera, C. F. Pirri,
P. Tiberto, M. Sangermano,
I. Roppolo,* G. Rizza 1900505

3D Printing of Magnetoresponsive Polymeric Materials with Tunable Mechanical and Magnetic Properties by Digital Light Processing

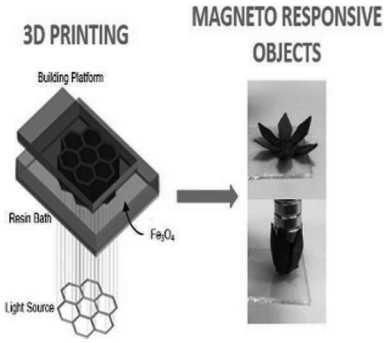

Digital light processing is used for 3D printing of magnetoresponsive polymeric materials with tunable mechanical and magnetic properties. Different objects are 3D printed varying stiffness and magnetic responses, probing different kinds of movements, such as rolling, translation, stretching, shape-shifting, and folding/unfolding under external magnetic fields.

ADVANCED MATERIALS TECHNOLOGIES
www.advmattechnol.de

3D Printing of Magnetoresponsive Polymeric Materials with Tunable Mechanical and Magnetic Properties by Digital Light Processing

Simone Lantean, Gabriele Barrera, Candido Fabrizio Pirri, Paola Tiberto, Marco Sangermano, Ignazio Roppolo,* and Giancarlo Rizza

In this work digital light processing is used for printing magnetoresponsive polymeric materials with tunable mechanical and magnetic properties. Mechanical properties are tailored, from stiff to soft, by combining urethane-acrylate resins with butyl acrylate as the reactive diluent. Moreover, the magnetic response of the printed samples is tuned by changing the Fe_3O_4 nanoparticle loading up to 6 wt%. Following this strategy, magnetoresponsive active components are fabricated with programmable complex functions using external magnetic fields. Different objects are printed varying stiffness and magnetic responses, probing different kinds of movements, such as rolling, translation, stretching, shape-shifting, and folding/unfolding.

1. Introduction

Bringing dynamics in 3D printed objects is nowadays one of the most important challenges for additive manufacturing: the ability to change the shape of 3D printed structures is also called 4D printing. 4D printing aims at exploiting advanced materials responding to external stimuli to program the actions of the printed objects.[1–4] Several stimuli-responsive materials—e.g., electroactive polymers,[5–7] hydrogels,[8–11] and nanocomposites[12–15]—have been investigated for a broad variety of applications, from micro- and soft-robotics[10,16–18] to biomedicine.[19–24] Among the different strategies, an accessible pathway to fabricate stimuli-responsive (4D) printed objects consists in magnetizing a soft-polymer by loading the polymeric matrix with magnetic fillers, such as particles of magnetite (Fe_3O_4) or neodymium–iron–boron (NdFeB).[25–31] Direct ink writing (DIW) and fused filament fabrication (FFF) have been used to fabricate fast responding actuators,[32,40] inks containing high loads of magnetic fillers[41] and 2D planar structures that exploit folding and unfolding processes.[42] Additionally, 3D printed permanent magnets were developed.[43–48]

However, both DIW and FFF present some drawbacks: first in terms of resolution; second in terms of the dispersion of the fillers, that may lead to nonhomogeneous magnetic response; and third in terms of temperature of processing, which could be not compatible with the fillers.[48,49] For the last one, the temperature can be decreased using some additives, however this approach may affect the mechanical performances of devices.[41]

An alternative to DIW and FFF is digital light processing (DLP). This vat polymerization 3D printing technology involves the use of photosensitive (liquid) resins which are able to cure (i.e., to solidify) upon irradiation with a suitable light source. In DLP, a digital light projector (digital micromirror device) illuminates a photocurable resin with a 2D pixel pattern allowing the curing of single slices of the 3D object.[50–52] The aforementioned drawbacks associated to DIW and FFF can be overcome by the use of DLP. Indeed: (i) the printing resolution in DLP belongs to the pixel dimensions and it is generally higher than DIW and FFF,[53,54] (ii) in DLP the dispersion of the fillers is easier to control since liquid formulations are used; and (iii) the fabrication process generally occurs at room temperature. Nevertheless, two precautions must be taken into account: first, the increase of the content of nanoparticles may affect the photopolymerization process since they compete with the photoinitiator in absorbing the incident radiation; and second, the dispersion of the fillers must be stable for the whole printing procedure in order to print an object whose response is homogeneous to an external input. For the latter, macroscopic sedimentation, segregation, and spatial inhomogeneity must be avoided.

S. Lantean, C. F. Pirri, M. Sangermano, I. Roppolo
Department of Applied Science and Technology
Politecnico di Torino
Corso Duca degli Abruzzi 24, 10129 Torino, Italy
E-mail: ignazio.roppolo@polito.it
S. Lantean, G. Rizza
Laboratoire des Solides Irradiés (LSI)
CEA/DRF/IRAMIS
Ecole polytechnique
CNRS
Institut Polytechnique de Paris
F-97728 Palaiseau, France
G. Barrera, P. Tiberto
Advanced Materials for Metrology and Life Sciences Division
INRiM
Strada delle Cacce 91, 10143 Torino, Italy
C. F. Pirri
Center for Sustainable Future Technologies @Polito
Istituto Italiano di Tecnologia
Via Livorno, 60, 10144 Torino, Italy
The ORCID identification number(s) for the author(s) of this article can be found under https://doi.org/10.1002/admt.201900505.

DOI: 10.1002/admt.201900505

Recently, some works have been published on the use of DLP to print magnetic nanocomposite materials. Among them, Martin et al.,[55] demonstrated the possibility to print bioinspired reinforced materials controlling the orientation of alumina platelets decorated with magnetite nanoparticles, while Ji et al. showed the possibility of printing multilayered magnetic soft-actuators containing 1 wt% of magnetite nanoparticles.[56]

Following this strategy, we applied DLP technology to fabricate magnetic responsive soft objects with programmable functions and magnetoresponsive active components.[32] Starting from our previous knowledge in polymer nanocomposites printing (see, e.g., refs. [57,58]), we optimized the photocurable formulation in terms of both reactivity and mechanical properties, achieving the desired mechanical properties and functional response. In particular, the mechanical response of the printed polymeric matrix was tailored from stiff to a flexible material by combining urethane-acrylate resins with butyl acrylate employed as the reactive diluent. Using optimized formulations and a visible light as a photocuring source, we were able to load the resin up to 6 wt% of magnetite nanoparticles. Finally, as a proof of concept, we have obtained a set of high-resolution 3D objects with complex shapes whose movements can be controlled by the application of an external magnetic field.

2. Results and Discussion

2.1. Optimization of the Photocurable Resin Containing Magnetic Nanofillers

Magnetoresponsive polymers were obtained by loading Ebecryl 8232 (100 Eb) resin with Fe_3O_4 nanofillers. A reactive diluent (butyl acrylate, BA) was added to tune the viscosity of the resins, the reactivity of the formulations toward light irradiation and the mechanical properties of the printed objects. As shown in **Figure 1**a), the addition of 25 wt% BA to pure Ebecryl (75Eb25BA), resulted in a decrease in the viscosity by one order of magnitude, i.e., from 5.06 to 0.18 Pa s. This value was further reduced by another order of magnitude when the concentration of BA was increased up to 50 wt% (50Eb50BA), i.e., at 0.02 Pa s. However, for higher concentrations of BA, the viscosity became so low that segregation/sedimentation effects made the formulations unstable and not suitable for our purposes. For all the formulations, the addition of magnetic nanofillers up to 8 wt% did not significantly affect the final viscosity (see Figure 1a). This unexpected result can be explained by considering the lubricant effect of spherical magnetite particles, which counterbalance the viscosity enhancement due to the dispersion of the fillers.[41]

Magnetite NPs dispersed within the formulations must be stable during the overall printing time in order to guarantee a homogeneous response of the printed objects; so, as otherwise stated, sedimentation and agglomeration must be avoided. Thus, the temporal stability of the embedded nanofillers was investigated. As a general result, we obtained that all formulations were stable, i.e., neither sedimentation nor agglomeration of the nanofillers was observed for at least 1 h, which is compatible with the printing process. As an example, in Figure S1, Supporting Information we show the stability of the formulation 50Eb50BA_6NP, which presents the lowest viscosity and the maximum amount of loaded Fe_3O_4 nanofillers, i.e., 6 wt%.

Next, we evaluated the photopolymerization reactivity of Ebecryl formulations modified by the presence of a reactive diluent (BA) and the magnetic nanofillers. In Figure 1b the double bonds conversions are reported as a function of irradiation time for different concentrations of the BA, i.e., 0 wt% (100 Eb), 25 wt% (75Eb25BA), and 50 wt% (50Eb350BA). The corresponding collected spectra are shown in Figures S2–S4, Supporting Information. The pristine Ebecryl resin (100 Eb) showed an overall double bond conversion of about 80% after 20 s. The 75Eb25BA formulation reached about 95% of conversion and it was accompanied by an enhancement of photopolymerization rate (initial slope of the curve). This phenomenon, also known as viscosity effect,[52,59] is associated to the presence of a low viscous reactive diluent that postpones the gelation point, which in turn accelerates the polymerization kinetics and increases the double bond conversions. However, when the BA content was further increased up to 50 wt%, not significant effects were appreciable, Figure 1b. Due to the higher reactivity, only the formulations containing BA are considered for the following investigations.

The influence of magnetic nanofillers (up to 8 wt%) on the polymerization process was evaluated by photorheology tests, by following the evolution of the storage moduli with

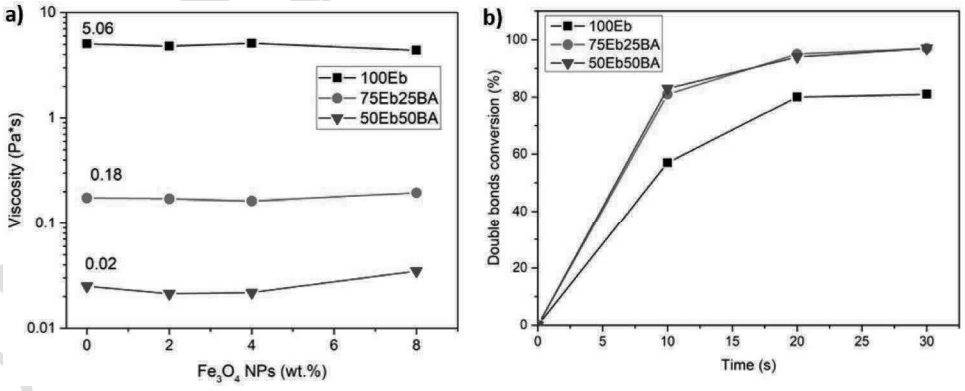

Figure 1. a) Influence of BA and NPs on formulation's viscosity. b) Double bond conversion VS irradiation time of 100 Eb, 75Eb25BA, and 50Eb50BA formulations.

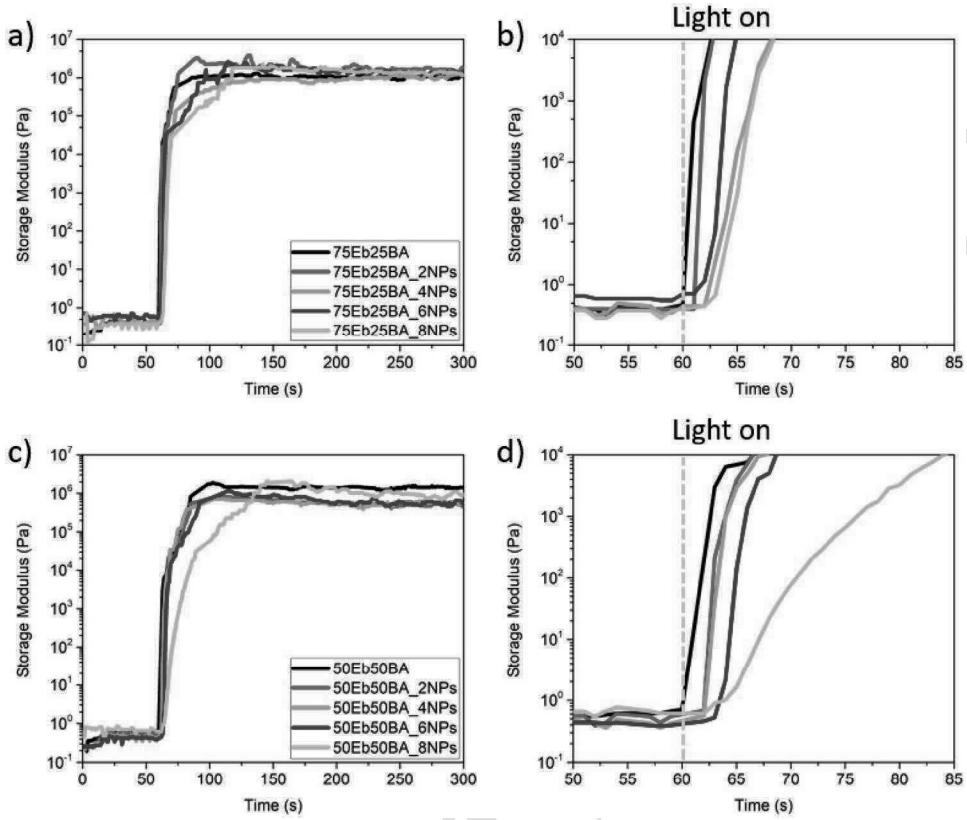

Figure 2. a) Photoreology tests performed on 75Eb25BA formulations. b) Zoom in during the first minutes of radiation of 75Eb25BA formulations. c) Photoreology tests performed on 50Eb50BA formulations. d) Zoom in during the first minutes of radiation of 50Eb50BA formulations.

the irradiation time. This is shown in **Figure 2**a,b for the 75Eb25BA-based formulations and in Figure 2c,d for the 50Eb50BA-based formulations. In agreement with FT-IR measurements, no appreciable differences between 75Eb25BA and 50Eb50BA formulations (without NPs) were observed. Indeed, in both cases, a fast photopolymerization process took place as soon as the light was switched on. On the other hand, the addition of Fe_3O_4 nanoparticles caused in both mixtures a slight delay in photopolymerization (see magnification of the starting point, Figure 2b,d, which scaled with the concentration of the nanofillers. This effect can be explained by considering the existence of a competitive absorption between the photoinitiator and the nanopowders. The efficiency of the radical photoinitiator is described by two quantum yields: the quantum yields of initiation, which represents the number of activated polymeric chains per absorbed photon, and the quantum yields of polymerization, which represents the number of monomer units polymerized per absorbed photon.[60–62] In presence of additional absorption sites, i.e., the ceramic nanofillers, the amount of the photons absorbed by the photoinitiator is reduced, which in turn leads to a decrease of the quantum yields and therefore to the slowing of the reaction kinetics. Despite the slight decrease of photoreactivity, increasing the amount of magnetic fillers in the objects it is possible to obtain response to lower magnetic field intensity: in this context, we 3D printed simple-shape objects (i.e., parallelepipeds) up to 8 wt% of nanofillers, and complex-shape object up to 6 wt% which is still a greater value compared to the recent literature (up to 1 wt%).[56] This could be explained considering that the absorption coefficient of magnetite NPs is lower in the visible (about 2×10^5 cm^{-1}) than in UV range (about 5×10^5 cm^{-1}).[63] It is important to highlight that the parameters extrapolated from photorheology experiments cannot be directly used for 3D printing procedure (e.g., irradiation time vs gel point), although those measurements give us useful indication for optimizing the printing process.

2.2. 3D Printing of the Optimized Photocurable Formulation and Material Characterization

First, to enhance the adhesion between the nanocomposite and the printing platform, a layer of polymer without nanofillers was preprinted. Then, formulations containing Fe_3O_4 NPs at increasing concentrations, up to a maximum of 8 wt%, were processed setting the thickness for each slice at 20 µm. The processing parameters are reported in **Table 1**. As expected, increasing the NPs content resulted in an increase of the irradiation time, following an exponential law (**Figure 3**a,b). Dataset can be fitted by the equation

$$y = A \cdot e^{x/t} + y_0 \quad (1)$$

The fitted curves were used to extrapolate the processing time and to check if it was compatible with the DLP (maximum irradiation time per layer 20 s). According to the interpolation curves, it could be possible to print nanocomposites containing

Table 1. Process parameters and glass transition temperatures of all studied formulations.

Sample	Slicing [µm]	Base exposing time [s]	Object exposing time [s]	T_g [°C]
100Eb	50	2.2	1.6	19.7
100BA		Not printable		−51.6(50)
75Eb25BA	50	2	1	4.3
75Eb25BA_2NPs	20	2.9	1.6	3.1
75Eb25BA_4NPs	20	4.4	2	3.3
75Eb25BA_6NPs	20	5.8	2.4	1
75Eb25BA_8NPs	20	9.5	3	−11
50Eb50BA	50	2	1	−6.2
50Eb50BA_2NPs	20	2.9	1.4	−8.4
50Eb50BA_4NPs	20	4.2	1.8	−7
50Eb50BA_6NPs	20	5.5	2.2	−10.7
50Eb50BA_8NPs	20	9.5	3	Not measured

up to 12 wt% of Fe_3O_4 NPs. However, taking into account that the mechanical resistance of the sample deteriorates with the increase of NPs concentration (see Figure 3c), we fixed the maximum amount of loaded magnetic nanofillers at 6 wt%.

Dynamic mechanical thermal analysis (DMTA) was used to evaluate the thermo-mechanical properties of the 3D printed samples. The influence of BA and Fe_3O_4 NPs on the glass transition temperature (T_g) of the 3D printed samples was determined (Table 1). The tanδ curves are shown in Figures S5 and S6, Supporting Information for the Eb75BA25 and Eb50BA50 formulations, respectively. On the one hand, when BA was added to the photocurable formulations, the T_g of the cross-linked material decreased. This softening effect is related to two phenomena: first a decrease of cross-linking density due to the presence of monofunctional monomers, second to the low T_g (about −51 °C) of the polybutylacrylate.[64] On the other hand, the T_g for the cross-linked material slightly decreased up to 4 wt% of magnetite nanoparticles, above this value the reduction of T_g was more evident. At first glance, this behavior can be ascribed to both the reduction of double bond conversion, in turn, related to the competitive absorption, and to the lubricating effect.[65]

Mechanical properties of the printed samples were evaluated by performing stress–strain tests on the printed objects using the 100 Eb specimens as reference. For the formulations without nanofillers, Figure 3c shows that the elastic moduli (E) decrease when BA was added, e.g., passing from 7 MPa for 100 Eb to 5.5 MPa for 75Eb25BA to 4.5 MPa for 50Eb50BA. For the nanocomposites, we observed a similar trend for both 75Eb25BA and 50EB50BA specimens. In fact, for both the formulations the values of E slightly decrease up to 6 wt% of nanofillers while above this value, a large drop of E was measured for 75Eb25BA samples.

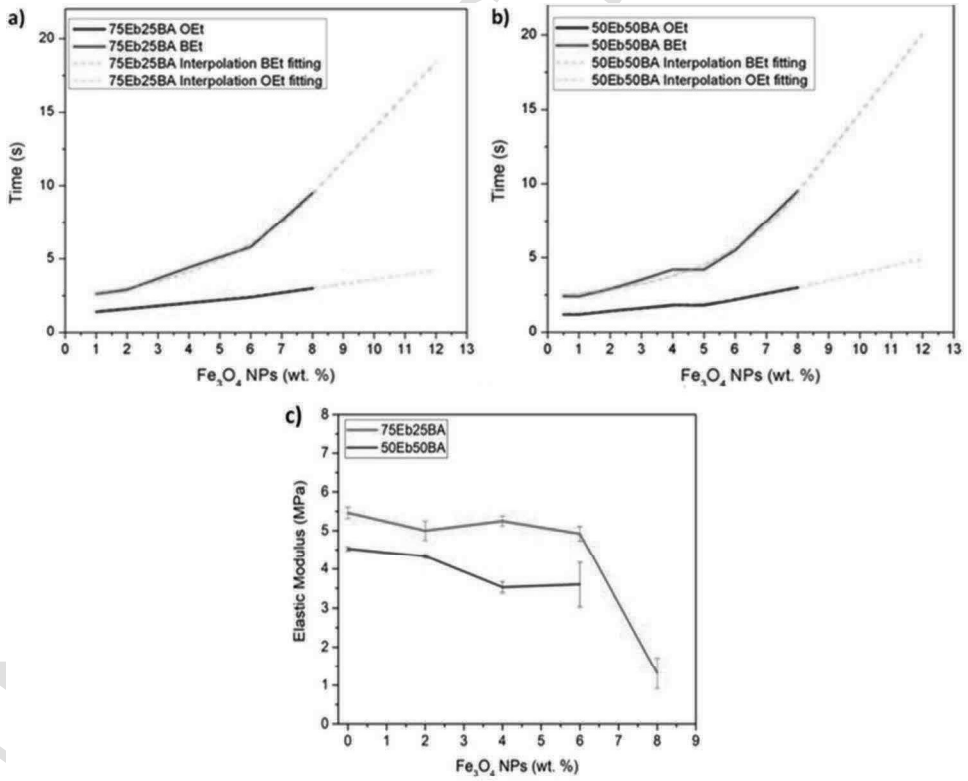

Figure 3. DLP processing parameters and their interpolation curves at several NPs concentrations of a) 75Eb25BA formulation and b) 50Eb50BA formulation. c) Elastic moduli trends when NPs concentrations are increased.

This is probably related to the defects produced during the manufacturing process. Moreover, the sample 50Eb50BA_8NPs was not printable due to its poor mechanical properties. Thus, by considering both mechanical properties and printing limitations, we set at 6 wt% the maximum concentration of nanofillers for the fabrication of our magnetoresponsive polymers.

The dispersion of the embedded magnetic nanoparticles was analyzed by optical and scanning electron (e.g., field emission scanning electron microscope, FESEM) microscopies (**Figure 4**). The optical analysis was performed on thin films, 12 µm thick, coated on a microscope slide by wire wound bar. FESEM images were taken on the cryofractured surfaces of 3D printed samples. To study the influence of viscosity on NPs dispersion, four systems were investigated: 75Eb25BA_2NPs, 75Eb25BA_8NPs, 50Eb50BA_2NPs, and 50Eb50BA_6NPs. In all the samples but 50Eb50BA, a homogeneous distribution of magnetite nanoparticles was observed. For the latter, some aggregates were visible, probably due to the low viscosity of this system, which made the homogeneous dispersions of the nanofillers difficult.

2.3. Magnetic Properties of the 3D Printed Samples

Room-temperature hysteresis loops are reported in **Figure 5**a,b for 75Eb25BA and 50Eb50BA samples, respectively, for different nanofiller concentrations. The latter value has been estimated by thermogravimetrical analysis (TGA) measurements (shown in Figures S7 and S8, Supporting Information). The magnetization (M) of the 3D printed nanocomposites was obtained by normalizing the magnetic moment to the sample mass. Magnetization curves displayed the same hysteretic and reversal behavior, fully compatible with Fe_3O_4 particles having 50–100 nm diameter and a multidomains state. As expected, M increases with increasing Fe_3O_4 content independently from the matrix formulation. This behavior is confirmed in Figure 5c for the two samples (75Eb25BA squares and 50Eb50BA circles), where a linear correlation between the value of M, taken at the maximum applied field (H = 17 kOe), and the nanoparticles concentration is observed. Besides, a coercivity value of ≈120 Oe has been recorded in all studied samples, indicating that the magnetic volume coherently responding to an external magnetic field H was substantially equal in the two classes of 3D printed polymers.[66] This result suggests a homogeneous distribution of Fe_3O_4 nanoparticles in the polymer matrix with a small fraction of NP aggregates confirming the analysis of optical and electronic images.

The magnetic force F_{mag} exerted on the magnetic polymer by applying an external magnetic field gradient to control the translation motion is given by

$$F_{mag} = MV\nabla H \quad (2)$$

where M is magnetization, V is the sample volume, and ∇H is the external field gradient.

The hysteresis curve maps the magnetic response as a function of the external magnetic field and consequently allows to figure out the F_{mag} intensity for all studied polymer concentration.

2.4. 3D Printing

X–Y plane resolution was characterized by printing holes and pillars of progressively smaller dimensions (**Figure 6**a–c). More complex objects, as honeycomb structures, were 3D printed to evaluate the CAD fidelity. Figure 6d,e) shows that the printed object reproduced with good fidelity the CAD file. Thus, we can state that the maximum resolution obtained for the formulations loaded with the highest amount of magnetite is about 400 µm. At last, to demonstrate the good toughness and flexibility of the final material, we printed thin films, 500 µm thick, and we show that it was possible to bend and twist them without damaging, regardless BA and NPs concentration (Figure S9, Supporting Information).

Finally, as a proof of concept, we printed a set of 3D objects with complex shapes, whose movements can be controlled by applying an external magnetic field. In particular, several types of motion have been investigated: (i) rolling, (ii) translation, (iii) stretching, (iv) shape-shifting, and (v) folding/unfolding. Rolling and translation are the easiest motions to exploit as they are related neither to mechanical properties nor to the shape-shifting of the material but only by the movement of the object as a whole. Thus, in this case, the use of soft and flexible polymeric matrices is not a stringent condition and the 75Eb25BA formulation, which gives stiffer objects, is perfectly suitable for our purposes. To study the rolling response to an external magnetic field, wheels (**Figure 7**c; Video S1, Supporting Information) and spheres (Figure 7d; Video S2, Supporting Information) have been printed. We noted that already at 2 wt% of nanofiller content, wheels and spheres underwent a rolling motion, which was controllable by changing the position of neodymium–iron–boron magnets (measured magnetic field of 300 mT). On the other hand, to exploit the translation movement, a cone-like feature was printed and placed in a tube filled with water (Figure 7e). As shown in Figure 7e and in Video S3, Supporting Information, the object can be remotely displaced by applying an external magnetic field.

On the other hand, stretching, shape-shifting, and folding/unfolding movements need printed materials to be somehow deformed, thus flexibility and softness, which are typical features of soft actuators, are mandatories. In order to produce soft actuators, 50Eb50BA matrix is preferable than 75Eb25BA matrix, since it shows lower values of elastic modulus (Figure 3c), cross-linking densities, and glass transition temperatures (Table 1). To study stretching movements, 50Eb50BA planar springs containing different concentrations of magnetite nanofillers have been printed (Figure 7a,b). As shown also in Videos S4 and S5, Supporting Information, when exposed to the same magnetic field (300 mT), the resin 50Eb50BA_6NPs (6 wt% of Fe_2O_3 NPs) shows a larger deformation amplitude than the resin 50Eb50BA_2NPs (2 wt% of $F_{e2}O_3$ NPs). This behavior has a twofold reason: on the one hand, the larger the load of magnetic nanoparticles, the larger the magnetization of the material and therefore the magnetic force between the printed item and the NdFeB magnets. On the other hand, as previously discussed, the softening of the material scales with the loading of nanofillers. Thus 50Eb50BA_6NPs materials will be more stretchable than 50Eb50BA_2NPs ones. Shapeshifting and folding/unfolding movements were investigated using

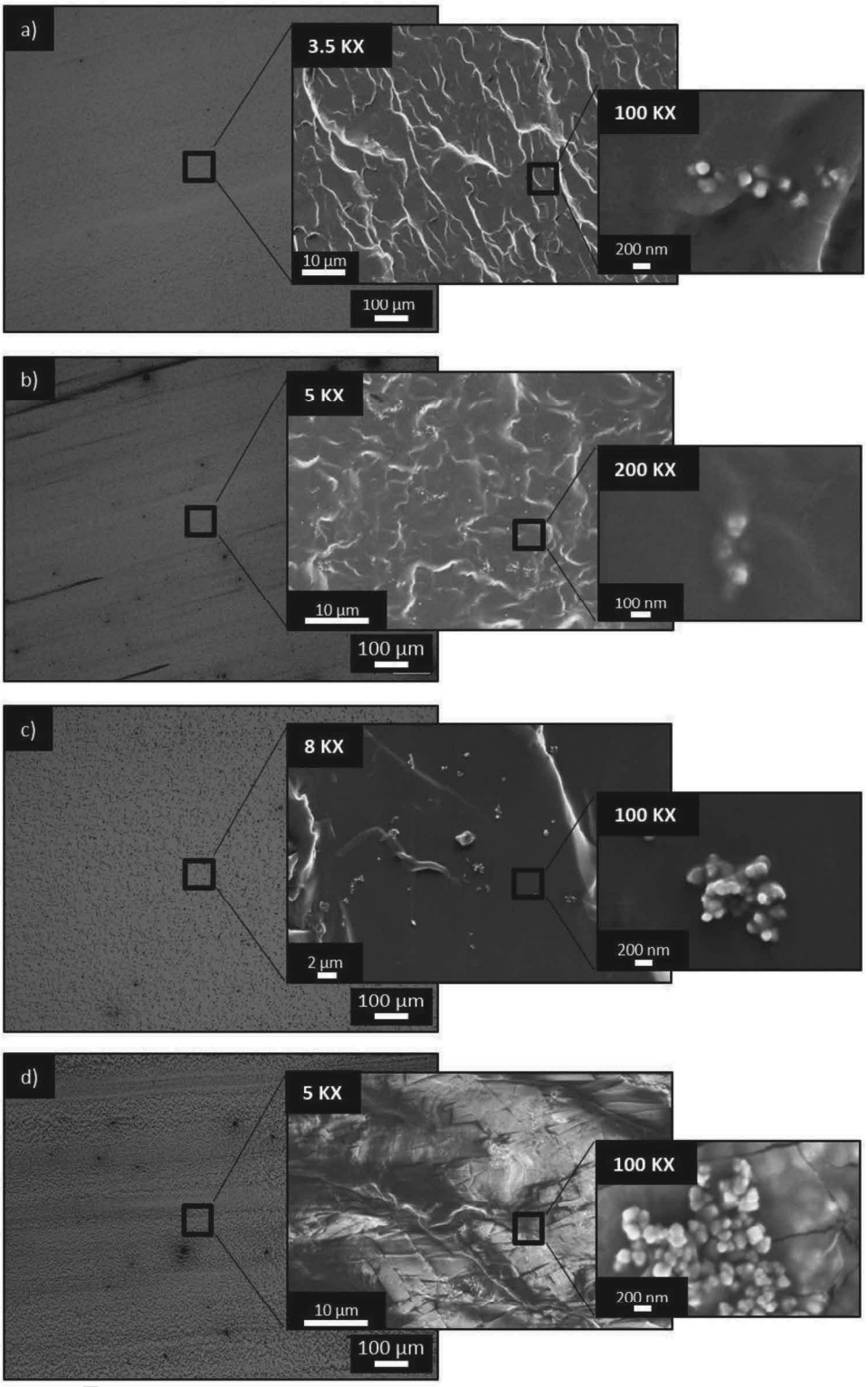

Figure 4. Optical microscope images taken of a) 75Eb25BA_2NPs, b) 75Eb25BA_8NPs, c) 50Eb50BA_2NPs, and d) 50Eb50BA_6NPs formulations. In the insets, FESEM images at different magnification values are reported.

50Eb50BA_6NPs formulation, as the printed material combines both high toughness and magnetomechanical response. A flower has been printed to check shape-shifting movement. Figure 7f and Video S6, Supporting Information show the blossom-like behavior of the printed flower when exposed to the magnetic field. This example is interesting for several

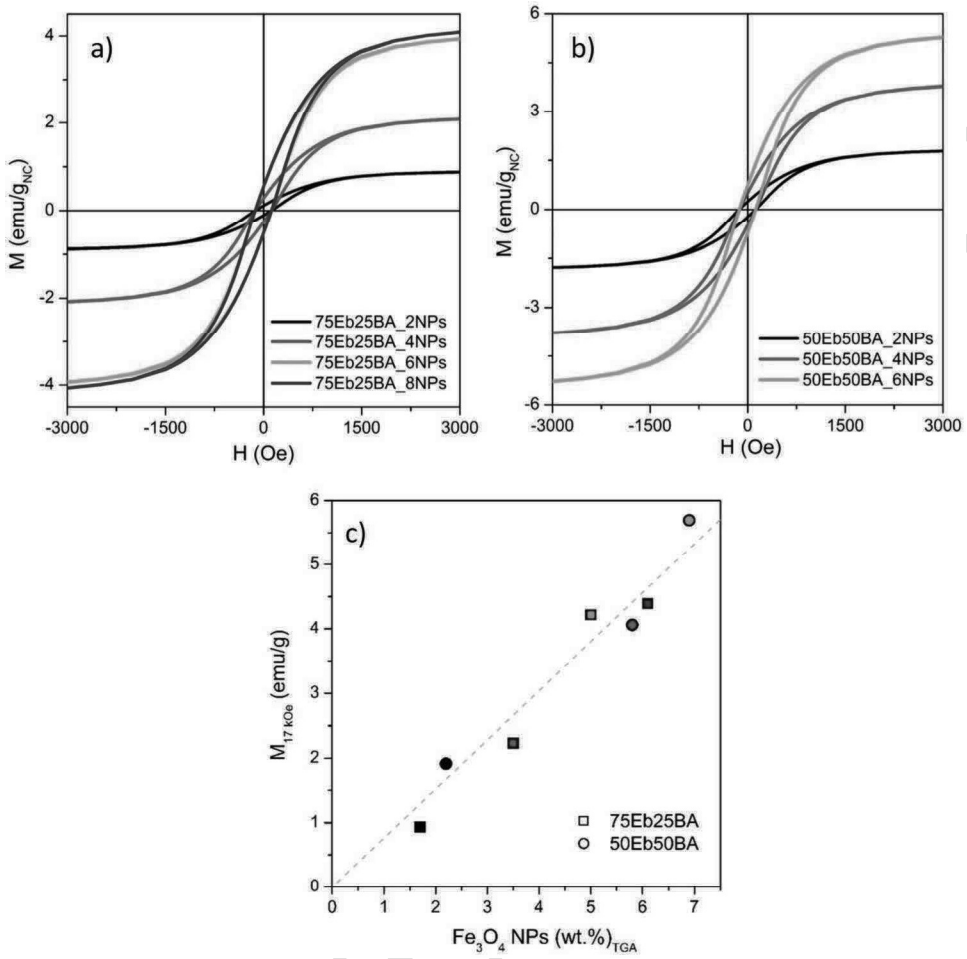

Figure 5. Room temperature hysteresis loops for a) 75Eb25BA and b) 50Eb50BA samples at different concentrations; evolution of magnetization (at $H = 17$ kOe) values for the 3D printed magnetic polymers (75Eb25BA squares and 50Eb50BA circles) as a function of Fe_3O_4 nanoparticles concentration estimated by TGA measurements (dotted line is a guide to the eyes).

engineering applications such as clamps or holders, as well as for industrial design applications.[56] Finally, the combination of polymers bonded magnetic nanofillers and pristine polymer matrices (without magnetic elements) allowed the fabrication of planar structures capable to transform through folding/unfolding movements into a 3D cube (Figure 7g; Video S7, Supporting Information). Here, pristine polymer elements were stuck to the magnetic structure to reinforce the walls of the cube during the folding/unfolding processes.

3. Conclusions

In this work we report on the fabrication of magnetoresponsive nanocomposite polymers using a DLP 3D printer. Photocurable urethane-acrylate resins were loaded with Fe_3O_4 nanoparticles. The mechanical properties of magnetoresponsive polymers were tailored, from stiff to soft, by combining urethane-acrylate resins with butyl acrylate, while the magnetic response of the samples was tuned by changing the nanoparticle loading. Moreover, we showed that magnetic properties are not affected by the polymer formulation and that the magnetization of the sample is simply proportional to the NPs concentration. The developed formulations were suitable for 3D printing and we were able to print with good resolution objects up to 6 wt% of nanomagnetite: the printed objects showed high-resolution details and fidelity compared to the CAD file. For higher NPs concentration, i.e., 8 wt%, the competition between the photoinitiator and the nanofillers in absorbing the light results in low reactivity and poor mechanical, not allowing an acceptable 3D printing process. Finally, several objects with a complex design were printed in 3D by adjusting their mechanical properties and magnetic responses to probe different kind of magnetic-controlled movements: (i) rolling, (ii) translation, (iii) stretching, (iv) shape-shifting, and (v) folding/unfolding.

This study goes in the direction to implement the light-driven printing techniques for the fabrication of high resolution magnetoresponsive 3D objects. The possibility to combine the accuracy of DLP with higher loads of magnetic nanofillers, may open the way to the 3D printing of magnetoresponsive items with a broad palette of advanced applications ranging from soft-robotics to biomedicine, from pharmaceutics to flexible electronics.

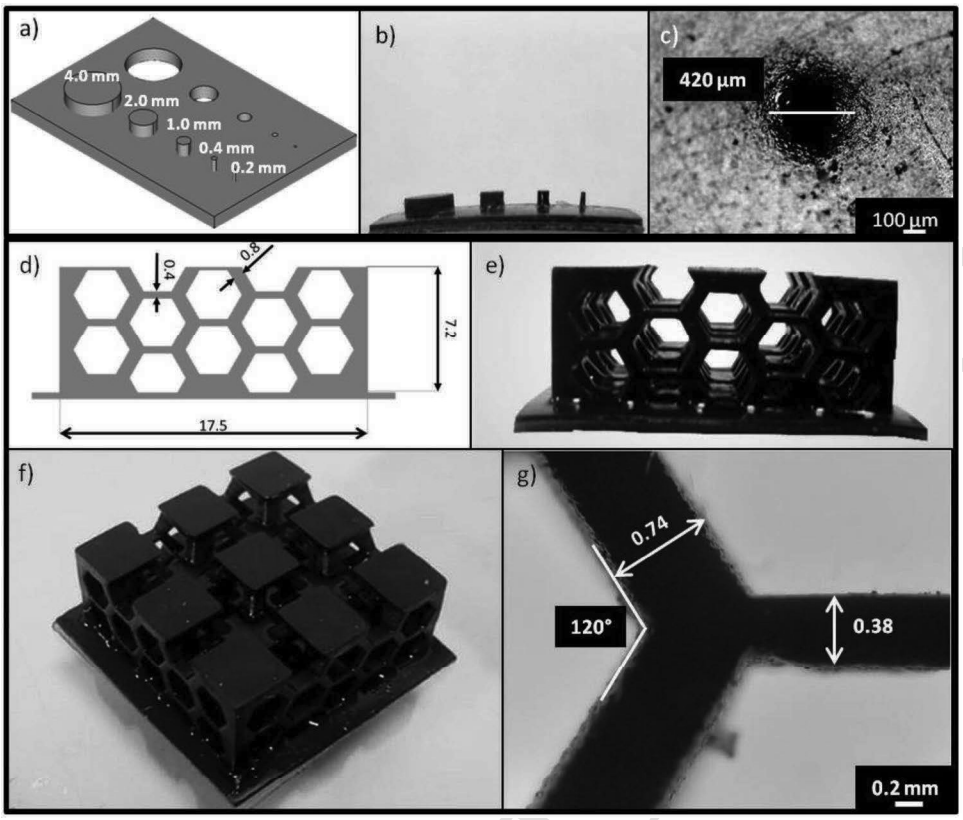

Figure 6. a) CAD design of the object used in order to determine *XY* resolution on the photocurable resin. b) Image of the corresponding printed object. c) Detail of the hole taken by optical microscope: scale bar is 100 µm. d) Honeycomb structure CAD file with quotations in mm. e) Lateral face of the printed object. f) Whole printed object. g) Detail of the hexagons taken with optical microscope: scale bar is 200 µm.

4. Experimental Section

Materials: Ebecryl 8232 (Eb), a urethane-acrylate resin, was kindly provided by Allnex. BA was purchased from Merck and added to Eb in several weight ratios as the reactive diluent. Phenylbis(2,4,6-trimethylbenzoyl)phosphine oxide (Merck) was added to the formulation as the photoinitiator at 1 wt% of the monomers. Spherical shape magnetite (Fe_3O_4) nanoparticles with a nominal diameter ranging between 50 and 100 nm (98% purity) were purchased from Merck and used as received.

Formulation Preparation: The formulations were prepared by varying the amount of the reactive diluent (BA) and the concentration of Fe_3O_4 nanoparticles (**Table 2**). BA was added to Ebecryl 8232 in three different weight concentrations (0%, 25%, and 50%), resulting in three different formulations named 100 Eb, 75Eb25BA, and 50Eb50BA, respectively. For each formulation, the concentration of the loaded Fe_3O_4 NPs was increased from 0 to 8 wt% relative to the amount of monomers. In the end, the photoinitiator was added to the formulation at 1 wt% of monomers amount. Formulations were then stirred and sonicated in order to disaggregate particles.

3D-Printed Sample Preparation: The formulations were 3D-printed using a RobotFactory HD 2.0 DLP printer equipped with a broadband projector emitting in the visible range, with 10 mW cm^{-2} of intensity and a nominal resolution of 50 µm in the *x*–*y* plane, while the maximum resolution in *z*-direction was 10 µm. In order to improve the adhesion of the printed structures to the building platform, a base-layer depleted of Fe_3O_4 NPs was fabricated before the printing of the final object. After samples cleaning, specimens underwent a UV postcuring for 10 min, using a medium-pressure mercury lamp also provided by RobotFactory.

Characterization: FT-IR spectra were collected using a Nicolet 50 FT-IR (Thermo Scientific). Formulations were coated on a silicon wafer using a wire wound bar, the film thickness was 12 µm. Samples were irradiated for 0, 10, 20, and 30 s using a Hamamatsu LC8 visible lamp with a cut-off filter below 400 nm, at the intensity of 10 mW cm^{-2} and under nitrogen flux. The conversion ratio of the acrylic groups was investigated monitoring the decrease of double-bond peak area in the range of 1630–1650 cm^{-1} during irradiation normalized with the aromatic peak area (1505–1575 cm^{-1}).

Rheological tests were performed with an Anton Paar rheometer (Physica MCR 302). The gap between the plates was settled at 0.2 mm, and the shear rate was varied from 0.1 to 100 1 s^{-1}. The same instrument was also used to perform photorheological tests. In this case, the machine was equipped with a Hamamatsu LC8 lamp having a cut-off filter below 400 nm and an intensity of 10 mW cm^{-2}. The gap between the plates was 0.2 mm; to stabilize the system, the light was switched on after 60 s. The tests were performed under constant temperature (25 °C) and shear frequency (1 rad s^{-1}).

DMTA was performed with Triton Technology TTDMA. 3D printed rectangular specimens (40 × 5 × 2 mm) were tested in strain control (0.02 mm of strain) with a frequency of 1 Hz, from –50 to 40 °C, with a heating ramp rate of 3 °C min^{-1}. Glass transition temperature (T_g) was set as the maximum of tanδ (= E''/E'). Stress–strain tests were performed with the same equipment to investigate the mechanical properties of the materials. For each formulation, four specimens were tested at room temperature, with a load rate of 1 N min^{-1}. TGA was made using a TGA/SDTA-851 (Mettler), testing ≈20 mg of sample. The measurements were performed in air atmosphere (50 mL min^{-1}) in the range of 25–800 °C with a heating rate of 10 °C min^{-1}. Two samples were tested for each formulation.

Optical microscopy images were taken with an Olympus BX53 M microscope. The ocular lenses and the objective lenses were equipped with 10× magnification.

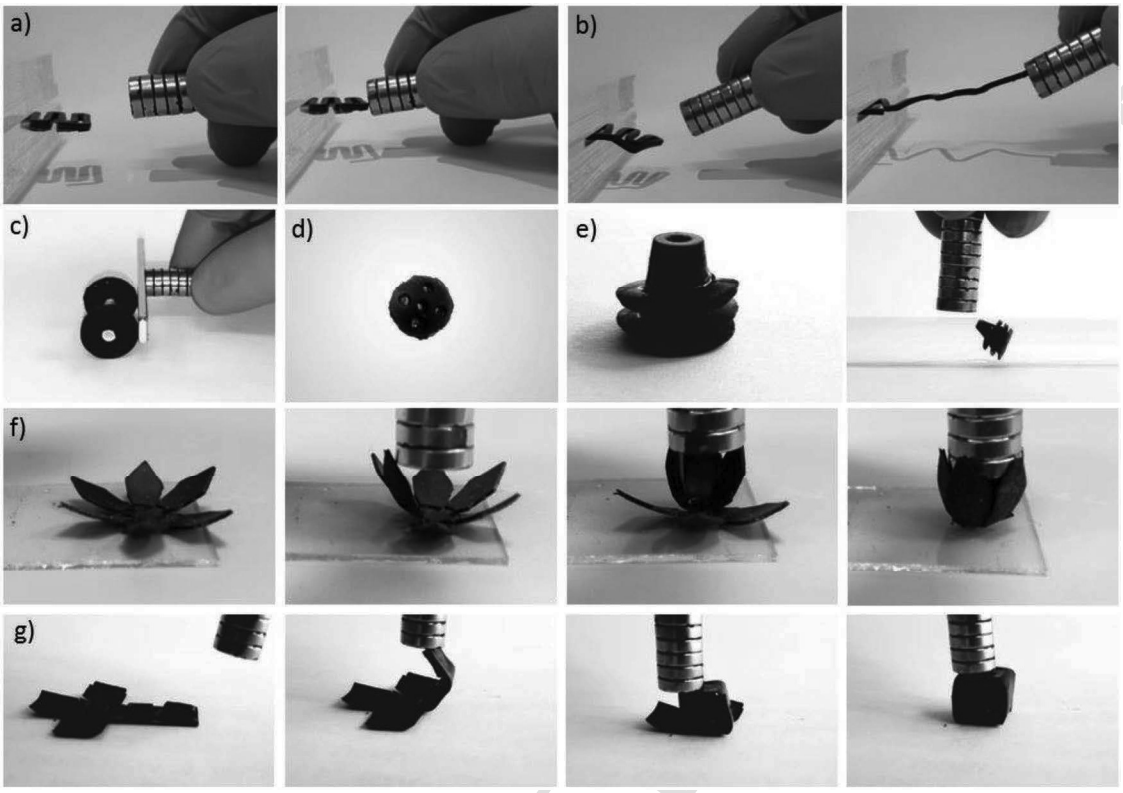

Figure 7. 3D printed magnetic objects. a) Printed spring with 2 wt% of magnetite. b) 3D Printed spring with 6 wt% of magnetite. c) Printed wheels. d) Printed sphere. e) Printed cone-like structure. f) Printed flower which encloses when exposed to a magnetic field. g) 2D structure composed of flexible and rigid elements able to create a 3D cube when exposed to a magnetic field.

FESEM (Zeiss Supra 40) is used to investigate the dispersion, distribution, and agglomeration of magnetite NPs in 3D printed samples changing their concentration and the viscosity of the former formulations. The investigated surfaces were obtained by cryofracture of the specimens.

Room-temperature hysteresis loops of 3D printed samples were measured by means of a vibrating sample magnetometer (Lakeshore 7400). The samples were mounted on a quartz sample-holder rod and submitted to a magnetic field (H) ranging in the interval -17 kOe $< H <$ 17 kOe. The magnetometer is routinely calibrated by means of a standard nickel sphere.

Q7 **Table 2.** Composition of the formulations.

Sample[a)]	Ebecryl 8232 [wt%]	Butyl acrylate [wt%]	Fe_3O_4 nanoparticles [wt% of monomers]
100Eb	100	–	0
75Eb25BA	75	25	0
75Eb25BA_2NPs	75	25	2
75Eb25BA_4NPs	75	25	4
75Eb25BA_6NPs	75	25	6
75Eb25BA_8NPs	75	25	8
50Eb50BA	50	50	0
50Eb50BA_2NPs	50	50	2
50Eb50BA_4NPs	50	50	4
50Eb50BA_6NPs	50	50	6
50Eb50BA_8NPs	50	50	8

[a)]All the formulations contained 1 wt% of the photoinitiator with respect to the amount of monomer.

Supporting Information

Supporting Information is available from the Wiley Online Library or from the author.

Acknowledgements

This work was supported by Compagnia di San Paolo through the funding scheme "Joint Project with Top Universities."

Conflict of Interest

The authors declare no conflict of interest.

Keywords

4D printing, digital light processing, magnetic materials

Received: June 14, 2019
Revised: September 13, 2019
Published online:

[1] X. Kuang, D. J. Roach, J. Wu, C. M. Hamel, Z. Ding, T. Wang, M. L. Dunn, H. J. Qi, *Adv. Funct. Mater.* **2019**, *29*, 1805290.
[2] A. Mitchell, U. Lafont, M. Hołyńska, C. Semprimoschnig, *Add. Manuf.* **2018**, *24*, 6060.
[3] S. Van Hoa, *Compos. Struct.* **2019**, *210*, 869.
[4] A. B. Baker, S. R. Bates, T. M. Llewellyn-Jones, L. P. Valori, M. P. Dicker, R. S. Trask, *Mater. Des.* **2019**, *163*, 107544.
[5] M. Layani, X. Wang, S. Magdassi, *Adv. Mater.* **2018**, *30*, 1706344.
[6] Y. Bar-Cohen, *J. Spacecr. Rockets* **2002**, *39*, 822.
[7] T. Mirfakhrai, J. D. W. Madden, R. H. Baughman, *Mater. Today* **2007**, *10*, 30.
[8] P. Calvert, *Adv. Mater.* **2009**, *21*, 743.
[9] Z. Liu, P. Calvert, *Adv. Mater.* **2000**, *12*, 288.
[10] S. Kim, C. Laschi, B. Trimmer, *Trends Biotechnol.* **2013**, *31*, 287.
[11] X. Peng, H. Wang, *J. Polym. Sci., Part B: Polym. Phys.* **2018**, *56*, 1314.
[12] A. Espinha, G. Guidetti, M. C. Serrano, B. Frka-Petesic, An. Dumanli, W. Y. Hamad, A. Blanco, C. López, S. Vignolini, *ACS Appl. Mater. Interfaces* **2016**, *8*, 31935.
[13] M. D. Lima, N. Li, M. J. De Andrade, S. Fang, J. Oh, G. M. Spinks, M. E. Kozlov, C. S. Haines, D. Suh, J. Foroughi, *Science* **2012**, *338*, 928.
[14] M. D. Lima, M. W. Hussain, G. M. Spinks, S. Naficy, D. Hagenasr, J. S. Bykova, D. Tolly, R. H. Baughman, *Small* **2015**, *11*, 3113.
[15] Z. Cheng, T. Wang, X. Li, Y. Zhang, H. Yu, *ACS Appl. Mater. Interfaces* **2015**, *7*, 27494.
[16] L. Hines, K. Petersen, G. Z. Lum, M. Sitti, *Adv. Mater.* **2017**, *29*, 1603483.
[17] P. Boyraz, G. Runge, A. Raatz, *Actuators* **2018**, *7*, 48.
[18] B. Gorissen, D. Reynaerts, S. Konishi, K. Yoshida, J. W. Kim, M. De Volder, *Adv. Mater.* **2017**, *29*, 1604977.
[19] T. Y. Dong, X. I. Zhang, T. Liu, *Front. Inf. Technol. Electron. Eng.* **2018**, *19*, 1303.
[20] C. Y. Chu, R. M. Patterson, *J. Neuroeng. Rehabil.* **2018**, *15*, 9.
[21] K. E. Peyer, L. Zhang, B. J. Nelson, *Nanoscale* **2013**, *5*, 1259.
[22] D. Grinberg, S. Siddique, M. Q. Le, R. Liang, J. F. Capsal, P. J. Cottinet, *J. Polym. Sci., Part B: Polym. Phys.* **2019**, *57*, 109.
[23] Y. S. Lui, W. T. Sow, L. P. Tan, Y. Wu, Y. Lai, H. Li, *Acta Biomater.* **2019**, *92*, 19.
[24] C. M. González-Henríquez, M. A. Sarabia-Vallejos, J. Rodriguez-Hernandeze, *Prog. Polym. Sci.* **2019**, *94*, 57.
[25] P. Allia, P. Tiberto, M. Coisson, A. Chiolerio, F. Celegato, F. Vinai, M. Sangermano, L. Suber, G. Marchegiani, *J. Nanopart. Res.* **2011**, *13*, 5615.
[26] T. Nardi, M. Sangermano, Y. Leterrier, P. Allia, P. Tiberto, J. A. E. Månson, *Polymer* **2013**, *54*, 4472.
[27] G. Barrera, P. Tiberto, P. Allia, B. Bonelli, S. Esposito, A. Marocco, M. Pansini, Y. Leterrier, *Appl. Sci.* **2019**, *9*, 212.
[28] J. Amici, P. Allia, P. Tiberto, M. Sangermano, *Macromol. Chem. Phys.* **2011**, *212*, 1629.
[29] J. Amici, M. Kahveci, P. Allia, P. Tiberto, Y. Yagci, M. Sangermano, *J. Mater. Sci.* **2012**, *47*, 412.
[30] A. Golbang, M. Kokabi, *Eur. Polym. J.* **2011**, *47*, 1709.
[31] A. Khosla, B. L. Gray, *ECS Trans.* **2012**, *45*, 477.
[32] Y. Kim, H. Yuk, R. Zhao, S. A. Chester, X. Zhao, *Nature* **2018**, *558*, 274.
[33] D. Kokkinis, M. Schaffner, A. R. Studart, *Nat. Commun.* **2015**, *6*, 8643.
[34] D. Sindersberger, A. Diermeier, N. Prem, G. J. Monkman, *Mater. Today Commun.* **2018**, *15*, 269.
[35] J. Pelteret, P. Steinmann, *Magneto Active Polymer: Fabrication, Characterisation, Modelling and Simulation at the Micro- and Macro-scale*, De Gruyter, Berlin **2019**.
[36] E. B. Joyee, Y. Pan, *Soft Rob.* **2019**, *6*, 333.
[37] C. De Marco, C. C. J. Alcantara, S. Kim, F. Briatico, A. Kadioglu, G. De Bernardis, X. Chen, C. Marano, B. J. Nelson, S. Panè, *Adv. Mater. Technol.* **2019**, *4*, 1900332.
[38] B. Khatri, K. Lappe, D. Noetzel, K. Pursche, T. Hanemann, *Materials* **2018**, *11*, 189.
[39] L. Lu, P. Guo, Y. Pan, *J. Manuf. Sci. Eng.* **2017**, *139*, 071008.
[40] A. Bastola, M. Paudel, L. Li, *Polymer* **2018**, *149*, 213.
[41] A. Hodaei, O. Akhlaghi, N. Khani, T. Aytas, D. Sezer, B. Tatli, Y. Z. Menceloglu, B. Koc, O. Akbulut, *ACS Appl. Mater. Interfaces* **2018**, *10*, 9873.
[42] H. Fu, K. Nan, W. Bai, W. Huang, K. Bai, L. Lu, C. Zhou, Y. Liu, F. Liu, J. Wang, *Nat. Mater.* **2018**, *17*, 268.
[43] C. Huber, C. Abert, F. Bruckner, M. Groenefeld, S. Schuschnigg, I. Teliban, C. Vogler, G. Wautischer, R. Windl, D. Suess, *Sci. Rep.* **2017**, *7*, 9419.
[44] J. Gandha, L. Li, I. C. Nlebedim, B. K. Post, V. Kunc, B. C. Sales, J. Bell, M. P. Paranthaman, *J. Magn. Magn. Mater.* **2018**, *467*, 8.
[45] E. M. Palmero, J. Rial, J. De Vicente, J. Camarero, B. Skarman, H. Vidarsson, *Sci. Technol. Adv. Mater.* **2018**, *19*, 465.
[46] E. M. Palmero, D. Casaleiz, N. A. Jiménez, J. Rial, J. de Vicente, A. Nieto, R. Altimira, A. Bollero, *IEEE Trans. Magn.* **2018**, *55*, 2101004.
[47] R. Domingo-Roca, J. C. Jackson, J. F. C. Windmill, *Mater. Des.* **2018**, *153*, 120.
[48] J. A. Cuenca, K. Bugler, S. Taylor, D. Morgan, P. Williams, J. Bauer, A. Porch, *J. Phys.: Condens. Matter* **2016**, *28*, 106002.
[49] J. H. Kim, S. Lee, M. Wajahat, H. Jeong, W. S. Chang, H. J. Jeong, J. Yang, J. T Kim, S. K. Seol, *ACS Nano* **2016**, *10*, 8879.
[50] F. P. W. Melchels, J. Feijen, D. W. Grijpma, *Biomaterials* **2010**, *31*, 6121.
[51] S. Lantean, I. Roppolo, M. Sangermano, C. F. Pirri, A. Chiappone, *Inventions* **2018**, *3*, 29.
[52] I. Roppolo, A. Chiappone, A. Angelini, S. Stassi, F. Frascella, C. F. Pirri, C. Ricciardi, E. Descrovi, *Mater. Horiz.* **2017**, *4*, 396.
[53] M. Hofmann, *ACS Macro Lett.* **2014**, *3*, 382.
[54] F. Frascella, G. Gonzalez, P. Bosch, A. Angelini, A. Chiappone, M. Sangermano, C. F. Pirri, I. Roppolo, *ACS Appl. Mater. Interfaces* **2018**, *10*, 39319.
[55] J. J. Martin, B. E. Fiore, R. M. Erb, *Nat. Commun.* **2015**, *6*, 8641.
[56] Z. Ji, C. Yan, B. Yu, X. Wang, F. Zhou, *Adv. Mater. Interfaces* **2017**, *4*, 1700629.
[57] A. Chiappone, I. Roppolo, E. Naretto, E. Fantino, F. Calignano, M. Sangermano, F. Pirri, *Composites, Part B* **2017**, *124*, 9.
[58] G. Gonzalez, A. Chiappone, I. Roppolo, E. Fantino, V. Bertana, F. Perrucci, L. Scaltrito, F. Pirri, M. Sangermano, *Polymer* **2017**, *109*, 246.
[59] M. Sangermano, W. Carbonaro, G. Malucelli, A. Priola, *Macromol. Mater. Eng.* **2008**, *293*, 515.
[60] K. D. Jandt, R. W. Mills, *Dent. Mater.* **2013**, *29*, 605.
[61] J. Fouassier, X. Allonas, D. Burget, *Prog. Org. Coat.* **2003**, *47*, 16.
[62] O. Valdes-Aguilera, C. Pathak, J. Shi, D. Watson, D. Neckers, *Macromolecules* **1992**, *25*, 541.
[63] A. Schlegel, S. F. Alvarado, P. Wachter, *J. Phys. C: Solid State Phys.* **1979**, *12*, 1157.
[64] M. Fernández–García, R. Cuervo–Rodriguez, E. Madruga, *J. Polym. Sci., Part B: Polym. Phys.* **1999**, *37*, 2512.
[65] C. Gao, Y. Wang, D. Hu, Z. Pan, L. Xiang, *J. Nanopart. Res.* **2013**, *15*, 1502.
[66] G. Herzer, *IEEE Trans. Magn.* **1990**, *26*, 1397.

